

NEAR-INFRARED SPECTROSCOPY OF BROWN DWARFS: METHANE AND THE TRANSITION BETWEEN THE L AND T SPECTRAL TYPES

Ian S. McLean¹,

L. Prato¹, Sungsoo S. Kim¹, M. K. Wilcox^{1,2}, J. Davy Kirkpatrick³, Adam Burgasser⁴

ABSTRACT

We report the possible identification of weak methane spectral features in the near-infrared K band in two late L dwarfs, DENIS 0205-11 (L7) and 2MASS 1523+30 (L8). New, high signal-to-noise ratio flux-calibrated spectra, spanning the wavelength interval 1.10 – 2.35 μm with an average resolving power $R = 1800$ were obtained using NIRSPEC on the Keck II telescope. Results are reported and compared for three late L dwarfs (L5, L7, and L8) and two T dwarfs (T1 and T6). The spectra, which are continuous through the atmospheric absorption bands, show the development of deep steam bands and the weakening of iron hydride features through the L dwarfs and the emergence of strong methane bands in the T dwarfs. A detailed comparison of the K band regions with synthetic spectra suggests that the weak features seen in the L7 and L8 dwarfs at 2.20 μm are likely to be methane. We see no evidence for methane in the H band. At the $R = 1800$ resolution, significant differences are evident between the spectral signatures of the L8 and the T1, leaving room for additional transition objects (L9 or T0).

Subject headings: infrared: stars — stars: low-mass, brown dwarfs

1. Introduction

Very low-mass stars and brown dwarfs with effective temperatures below ~ 2200 K exhibit complex spectra rich in molecular features. Many such objects have now been identified,

¹Department of Physics and Astronomy, University of California, Los Angeles, CA, 90095-1562

²Department of Physics and Astronomy, University of Hawaii, Hilo, HI, 96720

³Infrared Processing & Analysis Center, M/S 100-22, Caltech, Pasadena, CA 91125

⁴Division of Physics, Caltech, Pasadena, CA 91125

and the L and T classes, the first significant, new spectral classes in almost a century, have been added to the familiar OBAFGKM sequence (Kirkpatrick et al. 1999; Martín et al. 1999; Burgasser et al. 2001). Spectroscopically, the characteristics of L and T dwarfs are significantly different from late M dwarfs (Geballe et al. 1996; Ruiz et al. 1997; Tinney et al. 1997; Kirkpatrick et al. 1999; Reid et al. 2001; Burgasser et al. 2001). Titanium oxide and vanadium oxide bands lose their prominence in L dwarfs, revealing absorption by iron hydride (FeH) and chromium hydride. The alkali metals (Na, K, Rb, and Cs) become very strong and the pressure-broadened wings of these lines are a major opacity source at visible wavelengths (Burrows et al. 2000). In the infrared (IR), strong steam (H_2O) bands appear and become deeper in lower temperature objects. These IR H_2O bands can be used for spectral classification even at resolving powers of $R = \lambda/\Delta\lambda \sim 100 - 800$ (McLean et al. 2000; Reid et al. 2001; Testi et al. 2001; Burgasser et al. 2001), which is advantageous since brown dwarfs are much brighter at near-IR wavelengths. For example, for the L4 dwarf GD 165B, $I = 19.6$ mag but $K \sim 14$ mag (Zuckerman & Becklin 1992; Kirkpatrick et al. 1999). Classification as a T dwarf requires that strong methane (CH_4) absorption be present in the J , H and K bands (Kirkpatrick et al. 1999), although Noll et al. (2000) have shown that weak CH_4 appears in objects as early as L5 dwarfs when observed at the fundamental band at $\sim 3.3 \mu m$.

With the recent availability of powerful, new IR spectrometers on very large (8–10 m) telescopes, higher resolution spectroscopy of low-mass stars and brown dwarfs is now possible. In this paper we present new results from NIRSPEC, the first high-resolution cryogenic 1–5 μm spectrometer for the Keck II 10-meter telescope. This work is part of a larger survey (McLean et al. 2001) called the NIRSPEC Brown Dwarf Spectroscopic Survey (BDSS). The goals of the survey are (*i*) to obtain a consistent set of IR spectra with $R \sim 2000$ for a large sample of very low-mass stars and brown dwarfs for comparison with spectral energy distribution models, (*ii*) to obtain a set of very high-resolution spectra ($R \sim 20,000$) for detailed comparison of individual spectral features with model atmosphere predictions, and (*iii*) to monitor selected sources for Doppler shifts induced by unresolved binary companions.

In this paper, we present high signal-to-noise, flux-calibrated spectra covering 1.10–2.35 μm at a resolution of ~ 1800 for five objects spanning the transition between the L and T spectral types. We report the probable discovery of CH_4 features in the K band of L7 and L8 dwarfs. The observations, data reduction and calibration methods are described in §2. In §3 we present the new results and discuss their implications, with particular emphasis on the transition between the L and T classes. Section 4 is a summary of our conclusions.

2. Observations and Data Reduction

Table 1 lists the objects discussed in this paper and summarizes their photometric properties. Preliminary results for four of the objects were reported previously by Wilcox et al. (2000), but the data have been re-analyzed and flux-calibrated. The fifth object is an early T dwarf discovered by the Sloan Digital Sky Survey (Leggett et al. 2000). The L5 and L7 are non-lithium objects whereas the L8 is a lithium brown dwarf (Kirkpatrick et al. 1999, 2000). Four targets were observed in 1999 June–August, and one in 2000 December. The spectral types listed in Table 1 are from Kirkpatrick et al. (1999) and Burgasser et al. (2001).

The Keck II Near-IR Spectrometer, NIRSPEC, is a cross-dispersed, cryogenic echelle spectrometer employing a 1024×1024 ALADDIN InSb array detector (McLean et al. 1998, 2000). In echelle mode the resolving power is $\sim 25,000$ (2 pixels). A low-resolution mode of $R \sim 2000$ (2 pixels), can be obtained by replacing the echelle grating with a plane mirror. For the present study, we used the lower resolution mode to observe a broad wavelength span in the minimum number of grating settings and the shortest time. The total wavelength region covered was 1.10 – $2.35\mu\text{m}$, with a spectral resolving power of $R = 1800$ (6–13 Å resolution), corresponding to a slit width of $0.^{\prime\prime}38$ (2 pixels). Seeing conditions generally gave full-width half maximum values of $0.^{\prime\prime}5$ or better. The entire set of observations represents about 6 hours of on-source integration time. For each object, integrations of 600 s were taken at two nod positions, separated by $\sim 20''$ along the $42''$ slit. NIRSPEC’s IR slit-viewing camera was used frequently during the spectroscopic exposures to check centering on the slit while offset-guiding on a field star. Stars of spectral type A0 V – A2 V were observed at the same airmasses as the target objects to calibrate for absorption in the Earth’s atmosphere. Neon and argon arc lamp spectra, together with the spectrum of a flat field lamp and dark frames, were taken immediately after the observation of each source.

Since the NIRSPEC spectra are slightly curved and distorted by the high-throughput optics, it is necessary to correct for this effect before applying standard extraction techniques. We (S. S. Kim, L. Prato, and I. McLean) have developed software at UCLA to rectify the data and maximize the efficiency of the processing overall. This code utilizes the spectral traces of the bright early-type standard star and known arc lamp lines to map the distorted image to a spatially and spectrally linear, rectified image. First, the standard star (used to calibrate telluric atmospheric absorption), the target object, and the flat field (created by subtracting off the dark frame from the flat field lamp frame) images are cleaned, replacing bad pixels by interpolating over their neighbors. After rectification, the pairs of nodded target frames are subtracted to remove background and divided by the flat field. Comparison of the target spectrum with the OH night sky spectrum is used to detect artifacts caused by incomplete

subtraction and saturated OH lines. At this point, the power spectrum of each source is examined for evidence of fringing effects within the instrument; these effects are generally weak in the low-resolution mode. Spectra were extracted by summing ~ 10 adjacent rows, assuming that the noise is dominated by Poisson statistics. The same procedure is applied to the telluric standard star, except in this case any intrinsic stellar features, such as the Brackett and Paschen lines, are carefully removed from the spectra by interpolation. We then divide the target spectra by the corrected telluric standard spectra and multiply by a blackbody equivalent in temperature to that of the standard star (Cox 2000) to maintain the true form of the target spectra. Finally, the spectra produced from the two nod positions are averaged.

To flux-calibrate the data, we use 2MASS photometry except for the Sloan object, in which case the photometry is from Leggett et al. (2000) on the UKIRT system. Band-averaged flux densities for Vega are defined by

$$F_{\lambda}^{band}(\text{Vega}) \equiv \frac{\int F(\lambda; \text{Vega}) S(\lambda) d\lambda}{\int S(\lambda) d\lambda}, \quad (1)$$

where $F(\lambda; \text{Vega})$ is the flux density of Vega and $S(\lambda)$ is the transmission profile of a certain bandpass which is the product of detector quantum efficiency, filter transmission, optical efficiency, and atmospheric transmission. Band-averaged flux densities for targets are similarly defined:

$$F_{\lambda}^{band}(\text{target}) \equiv \frac{\int F(\lambda; \text{target}) S(\lambda) d\lambda}{\int S(\lambda) d\lambda}. \quad (2)$$

After removing the intrinsic telluric features, the flux density of the target is related to the data number count (after the whole reduction above), $D(\lambda)$, by a proportional coefficient c such that

$$F(\lambda; \text{target}) = c D(\lambda). \quad (3)$$

Using Vega to define zero magnitude at all wavelengths, the magnitude of the target at a given band becomes

$$\text{mag}(\text{target}) = -2.5 \log \frac{F_{\lambda}^{band}(\text{target})}{F_{\lambda}^{band}(\text{Vega})}. \quad (4)$$

Then one can flux-calibrate a spectrum by finding c from

$$c = \frac{\int S(\lambda) d\lambda}{\int D(\lambda) S(\lambda) d\lambda} F_{\lambda}^{band}(\text{Vega}) 10^{-0.4 \text{mag}(\text{target})}. \quad (5)$$

When using the 2MASS J , H , and K_s magnitudes for the flux-calibration, $S(\lambda)$ in the above equation is represented by the transmission profile of the 2MASS bandpasses, which we obtained from http://www.ipac.caltech.edu/2mass/releases/second/doc/sec3_1b1.html. Our

F_{λ}^{band} (Vega) values are based on data from Bergeron et al. (1995), kindly provided by D. Saumon, and the 2MASS filter set. We also compared these values to fluxes from Cohen et al. (1992), which are based on the UKIRT filter set and the atmospheric absorption at Kitt Peak (Cox 2000). A 5% difference was found in the J band, but only 1-2% difference in the H and K_s bands. For the flux calibration of the T1 dwarf, we used the IRACAM/UFTI J , H , and K filter bandpasses, available on the UKIRT website, with the F_{λ}^{band} (Vega) values from Cohen et al. (1992). The resulting spectra are shown in Figure 1. A gaussian smoothing function has been applied in this representation. Based on counting statistics, the signal-to-noise ratio is typically >100 . Except in the center of the deep H_2O bands where atmospheric transmission is poor, most of the small-scale structure in the spectra is real.

3. Results and Discussion

From Figure 1, it is evident that the absolute flux in the J band decreases relative to that in the H band from L5 – L8, presumably influenced by changes in dust opacity (Allard et al. 2001; Tsuji 2001; Marley & Ackerman 2001; Burrows et al. 2001), but recovers dramatically in the T dwarfs as the dust settles out below the photosphere. This effect is apparent in the $J - H$ colors of the objects; the L8 is clearly the reddest, with a $J - H$ of 1.32 (Table 1). H_2O bands deepen from L5–T5; the depth of these bands is a useful indicator of spectral class (McLean et al. 2000; Reid et al. 2001; Testi et al. 2001). A strong FeH band at $1.19\ \mu\text{m}$ weakens from L5 – L7 and is gone by L8. The equivalent widths of the neutral potassium lines (K I) change slightly as the lines at first weaken through L8 and then appear to increase in strength at T1 before declining again. At least part of the variation in the K I lines is a result of pressure-broadening and the apparent strengthening in lower temperature objects is likely caused by the different depth in the atmosphere that is reached when dust is absent (Saumon et al. 2000). At $2.295\ \mu\text{m}$, the CO $v=2-0$ bandhead is prominent through L8, but other CO transitions in this region are not. The presence of CH_4 in the early T dwarf (Leggett et al. 2000) produces distinct features in the J , H and K band spectra. In cooler objects such as the T6, these features develop into large absorption troughs easily detected in low resolution spectra. No evidence of the $4s^2S - 4p^2P^0$ doublet of Na I at $2.2076\ \mu\text{m}$ is apparent, even in our L5 spectrum. Although the opacity of this doublet is still strong for objects with $T_{eff} = 1600\ \text{K}$, it is insignificant in comparison to the continuum absorption by H_2O and H_2 , consistent with our non-detection (D. Saumon 2001, private communication).

Given the appearance of CH_4 in the late L dwarfs at $3.3\ \mu\text{m}$ (Noll et al. 2000; Geballe et al. 2001), we searched for CH_4 at shorter wavelengths. At the smoothed resolution of Figure 1

($R \sim 900$), there are features in the L7 and L8 dwarfs at $1.67 \mu\text{m}$ and $2.20 \mu\text{m}$, close to where CH_4 is expected to appear. The distinct H band line, prominent in Figure 2 at $\sim 1.669 \mu\text{m}$, is not the $2\nu_3 \text{CH}_4$ feature (Leggett et al. 2000) but rather an artifact of incomplete removal of a saturated OH night sky line (Cox 2000). These telluric lines may also be the source of similar features seen in the L dwarf spectra of Reid et al. (2001) and Burgasser et al. (2001). Our observations are compared to models with and without CH_4 opacity, kindly supplied by D. Saumon. The models shown in Figures 2 and 3 have $T_{\text{eff}} = 1500 \text{ K}$ with $\log(g) = 5$, solar metallicity, and $f_{\text{rain}} = 5$ (D. Saumon and M. Marley 2001, private communication; Ackerman & Marley 2001). CH_4 is present in the model near $1.667 \mu\text{m}$ but no corresponding feature is evident in the L dwarfs. The T1 dwarf does present a small absorption feature at $1.667 \mu\text{m}$ and a shallow, broad dip in the continuum from $\sim 1.665 - 1.675 \mu\text{m}$ (Figure 2). No differences were apparent, at a level greater than the average noise in our data, in the CH_4 and non- CH_4 models around the $1.32 \mu\text{m}$ region of the J band.

Figure 3 shows the expanded K band region. From $2.05 - 2.15 \mu\text{m}$ the dominant features are unresolved transitions of H_2O . There is excellent correspondence among the three L dwarfs in this region; most of the strongest features are also present in the T dwarfs, the coolest of which are well fit by models (Saumon et al. 2000; D. Saumon 2001, private communication). At the other end of the K band spectrum, the dominant feature is the CO band head at $2.295 \mu\text{m}$. On the long wavelength side of the band head, the flux increases slightly but fails to recover to the continuum level in the L5 dwarf. The later L types show only a decrease in flux at wavelengths longer than the CO bandhead, and for the T1, the CO absorption is blended with weak CH_4 . In general, for L dwarfs later than L5, there is a gradual decrease in flux beyond $2.15 \mu\text{m}$. This decrease has been attributed to collisionally induced absorption by H_2 (Ruiz et al. 1997; Tokunaga & Kobayashi 1999). When CH_4 absorption occurs, there is a break in the slope near $2.18 \mu\text{m}$ and a minimum develops at $2.2 \mu\text{m}$. This region is shown by the shaded area in Figure 3. The L7 and L8 spectra display a small break in the overall shape around $2.18 \mu\text{m}$. Sharp features appear near $2.20 \mu\text{m}$, analogous to the lines in the CH_4 opacity model. Even in the L5 dwarf spectrum a small feature at $2.2 \mu\text{m}$ suggests the presence of CH_4 . Hence, it appears that weak CH_4 absorption is present in the latest L dwarfs.

Clear differences between the L8 and T1 spectra at this resolution are evident in Figure 3. The L8 spectrum is more similar, both in overall shape and in individual features, to the L7. We therefore propose that identification of an additional subclass object, such as an L9 or a T0, would provide a smoother transition between the L and T dwarfs.

4. Conclusions

We have presented a consistent set of near-IR spectra, with a resolving power of $R = 1800$, for a sample of five objects cooler than $T_{eff} \sim 1600$. These data are part of our larger on-going spectroscopic survey. High-quality, flux-calibrated spectra from 1.13–2.33 μm are reported for three L dwarfs and two T dwarfs. We have used the higher spectral resolution to search for early evidence of the onset of CH_4 absorption in the late L dwarfs. By comparing the observations to spectra from synthetic model atmospheres with and without CH_4 opacity, we associate the 2.2 μm features with CH_4 indicating that methane first appears in dwarfs as early as L7 in the K band. The observations presented here show that the spectral distinction between L8 and T1 is significant at this resolution, therefore leaving room for additional transition objects.

It is a pleasure to acknowledge the hard work of past and present members of the NIRSPEC instrument team, without whose efforts these observations would not have been possible. It is also a pleasure to acknowledge CARA instrument specialists Tom Bida and David Sprayberry, in addition to the CARA staff and Keck II Observing Assistants for their exceptional support. We thank an anonymous referee for useful comments and suggestions which improved the manuscript. We are especially grateful to D. Saumon and M. Marley for extensive help and discussions about models, and for providing synthetic spectra. Data presented herein were obtained at the W.M. Keck Observatory, which is operated as a scientific partnership between the California Institute of Technology, the University of California and NASA. The Observatory was made possible by the generous financial support of the W.M. Keck Foundation.

REFERENCES

Ackerman, A. S., & Marley, M. S. 2001, *ApJ*, 556, 872

Allard, F., Hauschildt, P. H., Alexander, D. R., & Starrfield, S., 1997, *ARA&A*, 35, 137

Allard, F., Hauschildt, P. H., Alexander, D. R., Tamanai, A., & Schweitzer, A. 2001, *ApJ*, 556, 357

Bergeron, P., Wesamael, F., & Beauchamp, A. 1995, *PASP*, 107, 1047

Burgasser, A. J., et al. 2001, *ApJ*, 563, in press

Burrows, A., & Sharp, C. M. 1999, *ApJ*, 512, 843

Burrows, A., Marley, M. S., and Sharp, c. M. 2000, *ApJ*, 531, 438

Burrows, A., Hubbard, W. B., Lunine, J. I., & Liebert, J. 2001, *Rev. Mod. Phys.*, in press

Cohen, M., Walker, R. G., Barlow, M. J., & Deacon, J. R. 1992, *AJ*, 104, 1650

Cox, A. N., ed. 2000, *Allen's Astrophysical Quantities* (4th ed; New York: Springer)

Geballe, T. R., Kulkarni, S. R., Woodward, C. E., & Sloan, G. C. 1996, *ApJ*, 467, L101

Geballe, T. R., Noll, K. S., Leggett, S. K., Knapp, G. R., Fan, X., & Golimowski, D. 2001, in *Proceedings of the IAU Workshop on Ultracool Dwarfs: Surveys, Properties, and Spectral Classification* (Heidelberg: Springer-Verlag), in press

Kirkpatrick, J. D., et al. 1999, *ApJ*, 519, 802

Kirkpatrick, J. D., et al. 2000, *AJ*, 120, 447

Leggett, S. K., et al. 2000, *ApJ*, 536, L35

Marley, M. 1999, *PASP*, 111, 1591

Marley, M. S., & Ackerman, A. S. 2001, in *Proceedings of the IAU Symposium 202 on Planetary Systems in the Universe: Observation, Formation and Evolution* (ASP Conference Series), in press

Martín, E. L., Delfosse, X., Basri, G., Goldman, B., Forveille, T., & Zapatero-Osorio, M. R. 1999, *AJ*, 118, 2466

McLean, I. S., et al. 1998, *SPIE*, 3354, 566

McLean, I. S., et al. 2000, *SPIE*, 4008, 1048

McLean, I. S., et al. 2000, *ApJ*, 533, L45

McLean, I. S., et al. 2001, in preparation

Noll, K. S., Geballe, T. R., Leggett, S. K., & Marley, M. S. 2000, *ApJ*, 541, L75

Reid, I. N., et al. 2000, *AJ*, 119, 369

Reid, I. N., Burgasser, A. J., Cruz, K. L., Kirkpatrick, J. D., & Gizis, J. E. 2001, *AJ*, 121, 1710

Ruiz, M. T., Leggett, S. K., & Allard, F. 1997, *ApJ*, 491, L107

Saumon, D., et al. 2000, *ApJ*, 541, 374

Testi, L., et al. 2001, *ApJ*, 552, 147

Tinney, C. G., Delfosse, X., & Forveille, T. 1997, *ApJ*, 490, L95

Tokunaga, A. T., & Kobayashi, N. 1999, *AJ*, 117, 1010

Tsuji, T. 2001, in *Proceedings of the IAU Workshop on Ultracool Dwarfs: Surveys, Properties, and Spectral Classification* (Heidelberg: Springer-Verlag), in press

Wilcox, M. K., et al. 2000, *SPIE*, 4005, 296

Zuckerman, B., & Becklin, E. E. 1992, *ApJ*, 386, 260

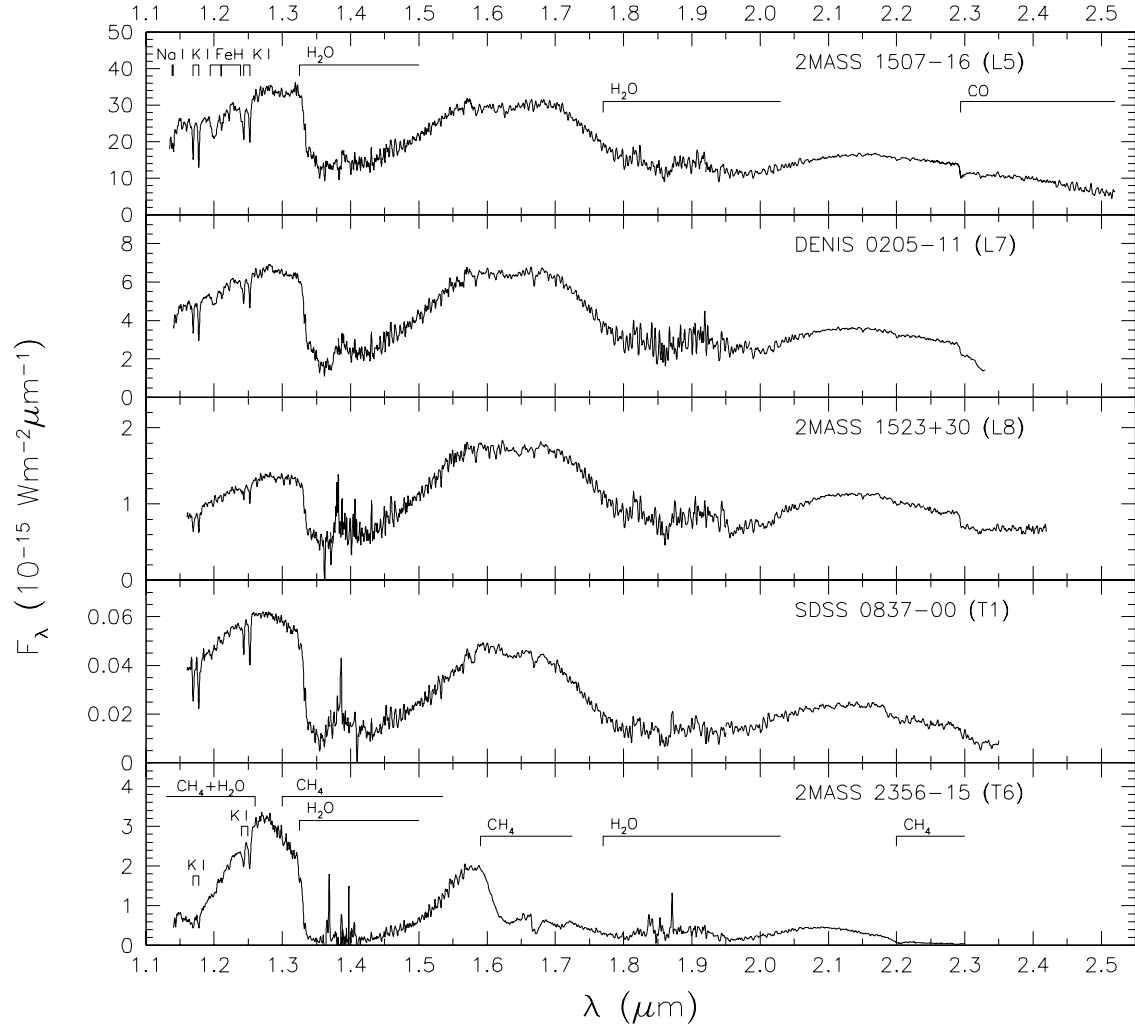


Fig. 1.— Flux calibrated near-infrared spectra of three L dwarfs and two T dwarfs obtained with NIRSPEC on the Keck II telescope. The original resolution ($R = 1800$) has been smoothed by a gaussian function of width 2 pixels, resulting in $R = 900$ in these plots. Some of the small, sharp features in the H band are attributable to saturated night sky OH lines (see text).

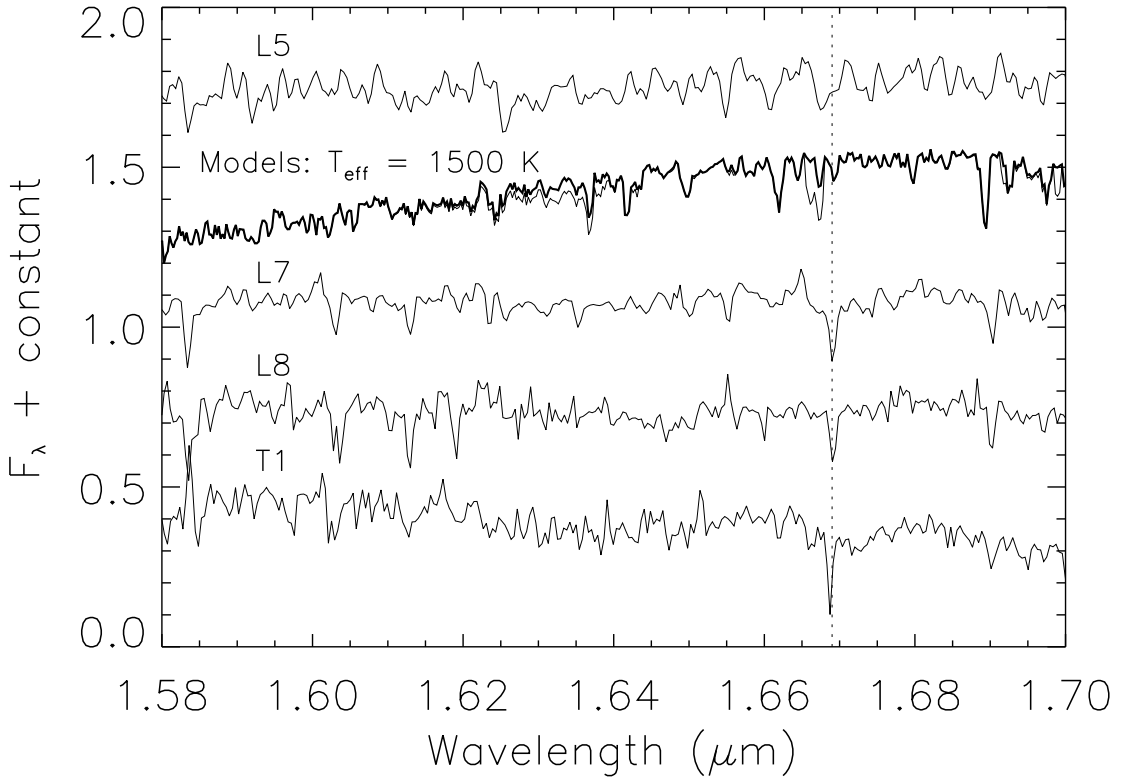


Fig. 2.— An expanded view of the *H* band region for the first four objects in Figure 1. The data are unsmoothed and $R = 1800$. Each spectrum has been normalized and offset by a constant. The dotted line indicates a spectral line associated with night sky OH near the $2\nu_3$ CH_4 feature. Also shown at similar resolution are two models (see text) courtesy of D. Saumon and M. Marley (2001, private communication), one with CH_4 opacity and one without (boldface). In the L dwarfs, we see no clear evidence of the $1.667 \mu\text{m}$ CH_4 feature present in the model. Although the OH line contamination is also present in the T1 dwarf, a small CH_4 line appears to be developing at $1.667 \mu\text{m}$ and a wider depression dips the continuum between 1.665 and $1.675 \mu\text{m}$.

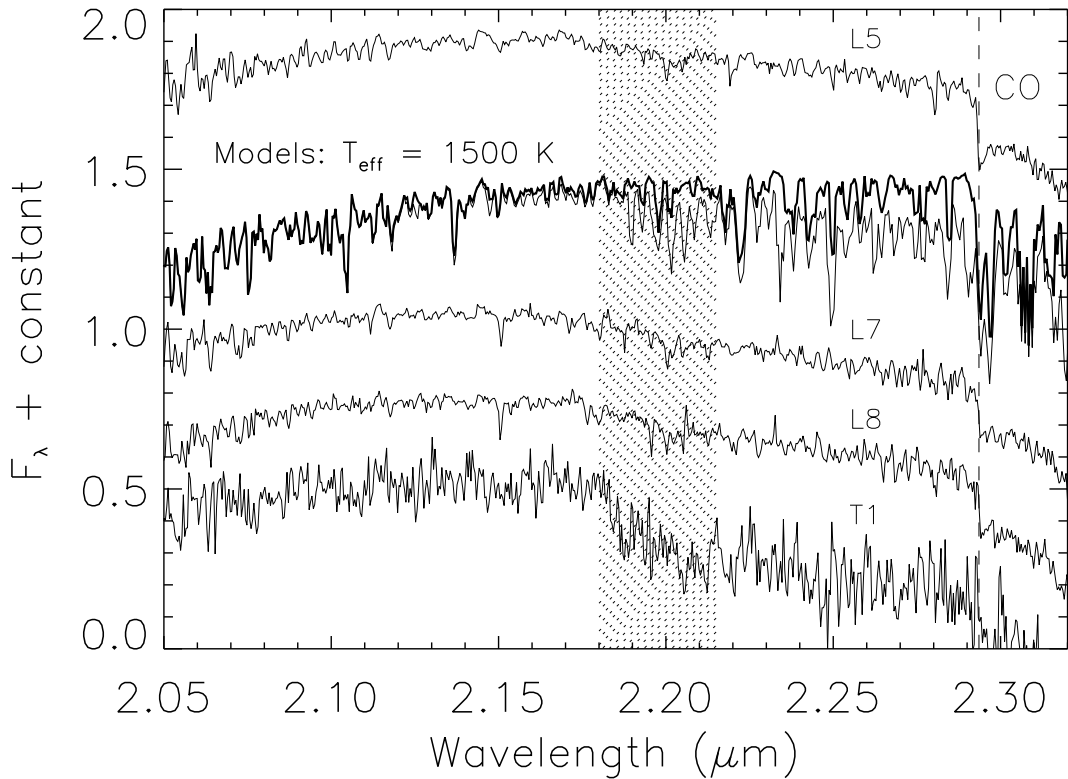


Fig. 3.— Similar to Figure 2 but for the K band region. The data are unsmoothed and $R = 1800$. Each spectrum has been normalized and offset by a constant. The shaded region indicates where CH_4 absorption first appears in the T dwarf. Also shown at similar resolution are two models (see text) with and without (boldface) CH_4 opacity. Incompletely removed night sky lines are again apparent at 2.195 and 2.150 μm . However, the most prominent CH_4 feature in the model, at 2.201 μm , a region unaffected by strong OH (Cox 2000), is clearly present in the L7 and L8 dwarfs. The continuum longward of 2.180 μm is strongly suppressed by CH_4 in the T1 dwarf. A small feature is present in the L5 dwarf at 2.2 μm ; possibly revealing the initial onset of CH_4 in brown dwarfs in the K band.

Table 1. Photometric Properties of the Observed Objects

Name	Spectral Type	J (mag)	H (mag)	K_s (mag)	Reference
2MASSI J1507476-162738	L5	12.82	11.89	11.30	1
DENIS-P J0205.4-1159	L7	14.55	13.59	12.99	2
2MASSW J1523226+301456 ^a	L8	16.32	15.00	14.24	1
SDSS J083717.21-000018.0 ^b	T1	16.90	16.21	15.98	3
2MASSI J2356547-155310	T6	15.80	15.64	15.83	4

^aAlso known as GL 584C

^bPhotometry on UKIRT system

Note. — References: (1) Kirkpatrick et al. (2000), (2) Kirkpatrick et al. (1999), (3) Leggett et al. (2000), (4) Burgasser et al. (2001)